École Polytechnique Fédérale de Lausanne

Towards replicating the full chewing process : Initial development of a Stewart platform-based chewing robot.

Master thesis

Author :

Barbara De Groot, 296815

CREATE Lab, Prof. Josie Hughes
Supervisor : Benhui Dai

June 11, 2025

Contents

1 Introduction

Human chewing is a complex process, involving different systems such as the jaw, teeth, tongue and saliva, all coordinated to break down food into a bolus that can be swallowed and digested. Chewing robots are a great tool to study this process that is not yet fully understood as they give us the opportunity for a closely controlled environment where each parameter can be adjusted and measured. This makes them valuable not only for advancing our understanding of chewing mechanics and related disorders, but also for a wide range of applications. In dentistry, they are used to test how implants and other dental devices wear over time. In food science, they help assess texture and flavor release during mastication. They also offer a reliable platform for studying the release of active compounds in chewable medications such as medical chewing gum.

Nowadays, many mastication robots exist, and while most are limited in their ability to fully mimic human chewing due to restricted degrees of freedom, some have already made significant progress. For example, the Bristol Dento-Munch Robo-Simulator [1] features 6 degrees of freedom (DoF), closed-loop control, force feedback, and a full set of teeth capable of replicating human chewing forces. Similarly, the robot developed by Seung-Ju Lee [2] offers the same capabilities, with a design that more closely follows human biomechanics. Another system, by Alemzadeh et al. [3], includes a closed mouth and artificial saliva—two important components of realistic mastication—even though it has limited sensory feedback. However, none of these systems combine all critical elements: 6 DoF, position and multidirectional force feedback, a closed mouth, and saliva. In addition, none of them include a tongue, which plays a crucial role in directing the food towards the molars and mixing it with saliva during chewing.

This project aims at developing a chewing robot that incorporates all these features, with the goal of replicating the full chewing process as closely as possible. As this is the first iteration, the focus is primarily on the mechanical design and the development of a simple, closed-loop, modular, and scalable control system that can be extended in future versions. The robot includes a 6-DoF Stewart platform capable of replicating chewing forces, along with tri-axial force sensing and position feedback to monitor jaw dynamics in detail. In parallel, we created a first dataset of human chewing motion using motion capture, as no publicly available datasets were found. This dataset will serve as a reference for identifying chewing patterns and improving control strategies. By laying down a flexible and expandable foundation, this work provides a platform for future integration of key components such as artificial saliva flow, an artificial tongue, and adaptive neuromuscular control strategies.

2 Methods

2.1 Design requirements from human physiology

The jaw makes essential contributions to the chewing process such as generating the forces required to break down food, controlling the lower mandible motion and giving sensory feedback. A robotic jaw should therefore be able to mimic these functions as closely as possible. As this is the first iteration of the chewing robot, we focus on force generation and range of motion, while sensory feedback and other functions can be added in future iterations. The design requirements are based on the literature and the human jaw anatomy and physiology, as summarized in Table 1. Note that the jaw's speed is not a design requirement as food can be effictively chewed even at slow speeds.

Quantity	**Values reported in the literature**	**Design requirement**
Degrees of freedom (DoF)	6 DoF: 3 translational (X, Y, Z) and 3 rotational (roll, pitch, yaw) [4]	6 DoF
Vertical (compressive) bite force F_z	600 N chewing force in healthy adults [5], 1243 N maximum clenching force [6]	800 N
Lateral force F_x	−72 N (left) to +53 N (right) during maximal biting [7]	±100 N
Anterior–posterior force F_y	−10 N (posterior) to +30 N (anterior) [7]	±50 N
Mandibular motion range	14 mm lateral shift, 11 mm protrusion, 61 mm mouth opening in healthy adults [8]	±20 mm (X, Y); 0–70 mm (Z)

Table 1: Functional design requirements.

2.2 Mechanical design

- choosing the dimensions of the stewart platform based on the size of the actuators + working space of the robot
- choice of structure/material to hold upper jaw to be rigid enough to not deform under the forces applied by the actuators
- 3 axis load cells to measure the force applied by the jaw
- so far 3d printed teeth/jaw but to be changed in the future

The first major design decision was how to achieve 6 degrees of freedom (DoF) for jaw motion. In the field of robotic mastication, two common approaches are used. The first is a biomechanically inspired design using linear actuators [2] or combinations of actuated cables and springs [3] to replicate muscle behavior. The second is a Stewart platform [1]—a widely used 6-DoF parallel mechanism, often seen in motion simulators. See Figure 1 for a visualization of the two approaches.

For this project, we chose the Stewart platform approach. Its well-defined kinematics and ease of control make it particularly suitable for our goal of replicating recorded human chewing motion.

Because our control strategy is based on reproducing real motion trajectories, having a platform with straightforward inverse kinematics is a key advantage.

Stewart platforms generally come in two configurations: one based on rotary servo motors and one based on linear actuators, see Figure 1. We selected the linear actuator design for several reasons. It offers more efficient force transmission, a simpler kinematic model, and greater structural rigidity—all important factors when attempting to reproduce the forces involved in human chewing.

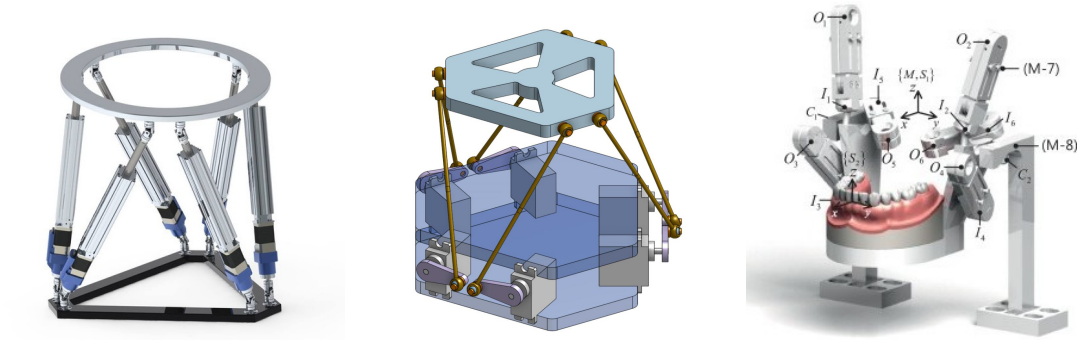

(a) **(b)** **(c)**

Figure 1: (a) Linear actuator-based jaw design. (b) Rotary servo motor-based Stewart platform. (c) Biomechanically inspired design[2].

The platform's dimensions were determined based on actuator specifications, desired jaw range of motion, and the working space required. The working space refers to the overall range of jaw motion and is defined by functional requirements summarized in Table 1. Based on findings in [9], we prioritized achieving the necessary vertical range of motion, knowing that sufficient horizontal range would follow.

Assuming a minimum actuator mounting angle of 45° to the horizontal, the minimum required stroke length is calculated as:

$$l_{\min} = \frac{z_{\max} - z_{\min}}{\sin(45°)} = \frac{70\,\text{mm}}{\sin(45°)} \approx 99\,\text{mm} \tag{1}$$

To meet the minimum vertical force requirement of 800 N, each actuator must provide:

$$F_{\min} = \frac{F_{z,\min}}{6 \cdot \sin(45°)} = \frac{800\,\text{N}}{6 \cdot \sin(45°)} \approx 189\,\text{N} \tag{2}$$

With this minimum actuator force, we estimate the lateral (shear) and front-back force capacities as:

$$F_x \approx 2 \cdot \cos(45°) \cdot F_{\min} + 4 \cdot \cos(45°) \cdot \sin(30°) \cdot F_{\min} \approx 534\,\text{N} \gg 100\,\text{N} \tag{3}$$

$$F_y \approx 4 \cdot \cos(45°) \cdot \cos(30°) \cdot F_{\min} \approx 462\,\text{N} \gg 50\,\text{N} \tag{4}$$

These calculations show that ensuring the vertical force requirement is met also guarantees that shear forces in the x and y directions will exceed their respective targets.

Since speed is not a strict requirement for this prototype, we prioritized force over velocity when selecting actuators. Position feedback is necessary for closed-loop control, as we use inverse kinematics to compute actuator positions based on the desired platform pose.

We selected the PA-14P-4-50 linear actuator, which meets both stroke and force requirements as seen in table 2.

Parameter	**Value**
Stroke length	101 mm
Max force	222.4 N
Speed (no load)	28 mm/s
Speed (full load)	21 mm/s
Position feedback	Potentiometer

Table 2: PA-14P-4-50 specifications.

2.3 Control

2.3.1 Hardware (electronics)

A Teensy 4.1 (600 MHz ARM Cortex-M7, single-precision FPU) executes the control loop.Its key peripherals are:

- three 12 A dual DC motor drivers (DF Robot) controlling the six linear actuators;
- six analogue inputs reading potentiometer position feedback from the linear actuators;
- three transmitters for the load cells mounted on top of the maxilla;
- an on-board micro-SD slot used for trajectory files and calibration data.

A 12 V AC/DC brick powers the actuators directly; the user's computer supplies 5 V to the Teensy, which in turn sources the 3.3 V logic rails for the motor drivers and load-cell transmitters. The full electronics schematic is shown in Fig. 2.

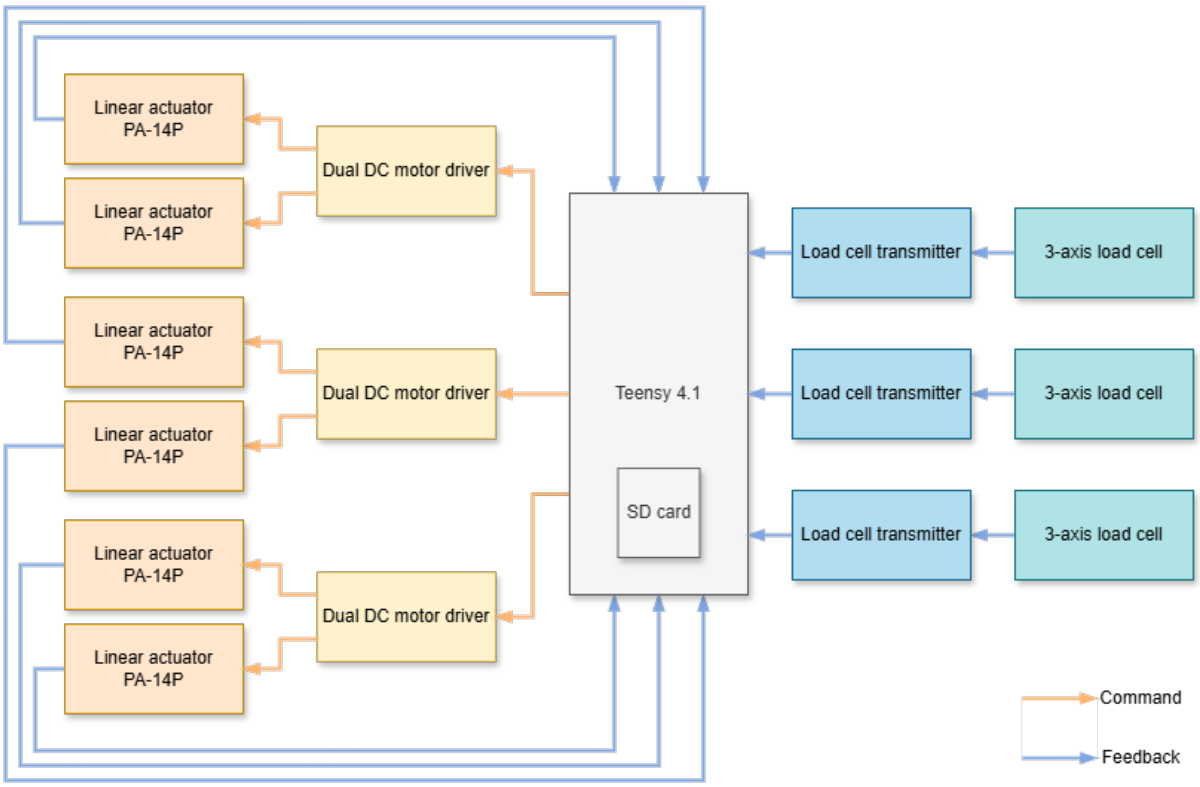

Figure 2: Electronics schematic.

2.3.2 Software architecture

The central class `RobotController` maintains the finite-state machine in Fig. 4 and manages two modules:

- `StewartPlatform`: inverse kinematics, trajectory interpolation, and low-level actuator commands;
- `ForceSensing`: continuous load-cell acquisition and filtering;

The controller is designed to be modular, allowing for easy addition of new modules such as a tongue or saliva module in the future. The three controller states are:

1. **Stop** – return to home pose; reload trajectory if the user selects a new file;
2. **Calibrate** – user can manually change the initial (x, y, z) position via the GUI;
3. **Move** – replay the selected trajectory.

A lightweight Python GUI on the host PC issues high-level commands, such as state changes, and plots sensor data.

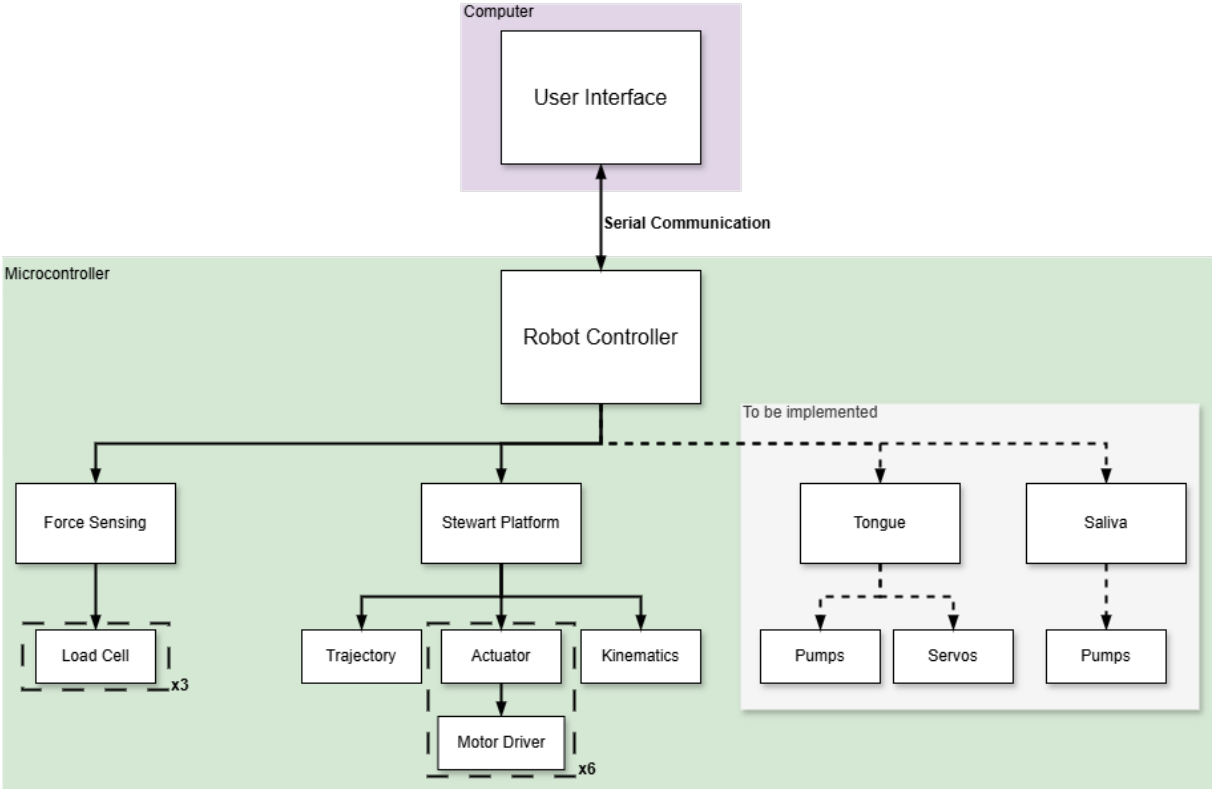

Figure 3: Overall code structure.

Figure 4: Robot controller state machine.

2.3.3 Position control

The Stewart Platform follows a 3D trajectory (x, y, z, roll, pitch, yaw) from a .csv file on the micro-SD card. See section 2.4 for details on the recording protocol and data processing. Each pose is defined by its position $\mathbf{t} = (x, y, z)$ and orientation given by the Euler angles (ϕ, θ, ψ), which are the roll, pitch, and yaw angles respectively. The trajectory is then linearly interpolated with a fixed time step chosen by the user.

Inverse kinematics For each pose in the trajectory, `Kinematics` computes the lengths of the six linear actuators that will achieve the desired pose of the platform, i.e. the inverse kinematics. To do so, we first compute the standard rotation matrix $R(\phi, \theta, \psi)$ for the Euler angles, which is defined as the product of three rotation matrices about the Z, Y, and X axes:

$$R(\phi,\theta,\psi) = R_Z(\psi)R_Y(\theta)R_X(\phi) = \begin{pmatrix} \cos\psi & -\sin\psi & 0 \\ \sin\psi & \cos\psi & 0 \\ 0 & 0 & 1 \end{pmatrix} \begin{pmatrix} \cos\theta & 0 & \sin\theta \\ 0 & 1 & 0 \\ -\sin\theta & 0 & \cos\theta \end{pmatrix} \begin{pmatrix} 1 & 0 & 0 \\ 0 & \cos\phi & -\sin\phi \\ 0 & \sin\phi & \cos\phi \end{pmatrix}$$

The platform joints $\mathbf{p}_i$, i being the actuator index, are then rotated about a fixed point $\mathbf{c}$, which is the front of the gnathion, and translated by the user-defined home position $\mathbf{t} = (x, y, z)$,

resulting in the world coordinates of the platform joints:

$$\mathbf{w}_i = R(\mathbf{p}_i - \mathbf{c}) + \mathbf{c} + \mathbf{t}.$$

Finally, the actuator length is the Euclidean distance to the fixed base joint $\mathbf{b}_i$:

$$\ell_i = \|\mathbf{w}_i - \mathbf{b}_i\|_2.$$

PI controller For each actuator, its desired length is sent to a PI position controller, see Figure 5. To minimize the noise of the potentiometer feedback, we apply a low-pass filter averaging the last 10 samples.

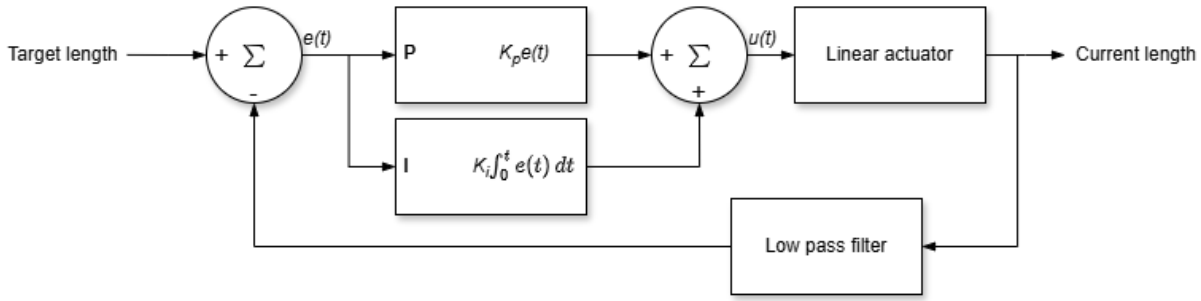

Figure 5: Position PI controller for the linear actuators.

2.4 Data acquisition and processing

Subjects. Two healthy adult volunteers (author and project supervisor) participated in this pilot recording. Owing to time constraints and the exploratory nature of the study, no additional subjects were recruited.

Motion-capture acquisition. Mandibular motion was recorded with a five-camera OptiTrack system sampling at 120 Hz. Four reflective markers arranged in a square were attached to the forehead and served as a head-fixed reference frame. A second set of three markers forming a triangle was placed on the gnathion. Two additional lip markers were recorded but later discarded because a single marker cannot encode orientation. [10, 11]

The subject then performed the motion sequences listed in Table 3. Each frame was saved by Motive as a `.csv` file that contains the 3-D marker positions (in millimetres) and the orientation of each marker set as quaternions. The calibrated volume had a residual error of 0.3 mm.

Food	**Motion**	***Optional:* Duration**
Empty mouth	20× open–close cycles	—
Chewing gum (Xylit-Pro, *Excitemint*)	Random side chewing	2 min
	Right-side chewing	1 min
	Left-side chewing	1 min
	Front-teeth-only chewing	1 min
Biscuits (Bretzeli, *Kambli*)	random chewing	—
	front-teeth chew → right-side chew	—
	front-teeth chew → left-side chew	—
	fast random chewing	—
	slow random chewing	—

Table 3: Recording protocol. *Notes:* For chewing-gum trials the first run began with an unchewed piece and the same gum was kept for all subsequent motions. For biscuit trials each run started with an empty, closed mouth; the subject then placed a biscuit, chewed as instructed, and swallowed.

Data processing. To reduce the noise, we apply a 4th-order butterworth filter to the data. The cutoff frequency is set to 6Hz, as human mastication frequency is around 1Hz to 2Hz . The data is then transformed to the head reference frame using rotation matrices.

3 Results

3.1 Mimicking human jaw motion

- human jaw motion from motion capture
- results of PCA on human jaw motion
- show graphs of human jaw motion vs robotic jaw motion
- show graphs of the force during chewing for human vs robot

3.2 chewing force

- max force that can be applied by the robot (both vertical and shear)
- show the force applied by the robot during chewing ?
- show the force applied by the human during chewing
- show the difference between the two

4 Discussion

4.1 Summary of findings

4.2 limitations

- So far very big and heavy robot due to steel plates and big actuator $\neq$ human jaw
- 3D printed teeth/jaw not strong enough to withstand the forces applied by the actuators

4.3 Future work

- 3D printed jaw/teeth to be replaced by a more rigid material
- add a tongue module
- add a saliva module
- adapt state machine to coordinate the different modules
- add a camera to track the food

5 Conclusion

6 References

[1] K Alemzadeh and D Raabe. "Prototyping artificial jaws for the Bristol Dento-Munch Robo-Simulator; 'A parallel robot to test dental components and materials". English. In: (2007). ISBN: 9781424407873 Name and Venue of Conference: 29th Annual International Conference of the IEEE Engineering in Medicine and Biology Society - Lyon, France Conference Organiser: IEEE, EMBS, SFGBM, pp. 1453–1456. DOI: 10.1109/IEMBS.2007.4352574.

[2] Seung-Ju Lee et al. "Design of mastication robot with life-sized linear actuator of human muscle and load cells for measuring force distribution on teeth". In: *Mechatronics* 51 (2018), pp. 127–136. ISSN: 0957-4158. DOI: https://doi.org/10.1016/j.mechatronics.2017.11.013. URL: https://www.sciencedirect.com/science/article/pii/S0957415817301769.

[3] Kazem Alemzadeh et al. "Development of a Chewing Robot with Built-in Humanoid Jaws to Simulate Mastication to Quantify Robotic Agents Release from Chewing Gums Compared to Human Participants". English. In: *IEEE Transactions on Biomedical Engineering* 68.2 (Feb. 2021), pp. 492–504. ISSN: 0018-9294. DOI: 10.1109/TBME.2020.3005863.

[4] Johannes H. Koolstra. "Dynamics of the Human Masticatory System". In: *Critical Reviews in Oral Biology & Medicine* 13.4 (2002), pp. 366–376. ISSN: 1045-4411. DOI: 10.1177/154411130201300406. URL: https://doi.org/10.1177/154411130201300406.

[5] K.C. Julien et al. "Normal masticatory performance in young adults and children". In: *Archives of Oral Biology* 41.1 (1996), pp. 69–75. ISSN: 0003-9969. DOI: https://doi.org/10.1016/0003-9969(95)00098-4. URL: https://www.sciencedirect.com/science/article/pii/0003996995000984.

[6] Charles H. Gibbs et al. "Maximum clenching force of patients with moderate loss of posterior tooth support: A pilot study". In: *The Journal of Prosthetic Dentistry* 88.5 (2002), pp. 498–502. ISSN: 0022-3913. DOI: https://doi.org/10.1067/mpr.2002.129062. URL: https://www.sciencedirect.com/science/article/pii/S0022391302002585.

[7] Sarah C. Woodford et al. "Muscle and joint mechanics during maximum force biting following total temporomandibular joint replacement surgery". In: *Biomechanics and Modeling in Mechanobiology* 23.3 (2024), pp. 809–823. ISSN: 1617-7959. DOI: 10.1007/s10237-023-01807-1. URL: https://doi.org/10.1007/s10237-023-01807-1.

[8] Vassil Svechtarov et al. "Mandibular range of motion and its relation to temporomandibular disorders". In: *Scripta Scientifica Medicinae Dentalis* 1.1 (2015).

[9] Oren Masory and Jian Wang and. "Workspace evaluation of Stewart platforms". In: *Advanced Robotics* 9.4 (1994), pp. 443–461. DOI: 10.1163/156855395X00508. eprint: https://doi.org/10.1163/156855395X00508. URL: https://doi.org/10.1163/156855395X00508.

[10] Steven Mills et al. "Principal Component Representations of Chewing Motion". In: IVCNZ '14 (2014), pp. 218–223. DOI: 10.1145/2683405.2683434. URL: https://doi.org/10.1145/2683405.2683434.

[11] Meg Simione et al. "Differing structural properties of foods affect the development of mandibular control and muscle coordination in infants and young children". In: *Physiology & Behavior* 186 (2018), pp. 62–72. ISSN: 0031-9384. DOI: https://doi.org/10.1016/j.physbeh.2018.01.009. URL: https://www.sciencedirect.com/science/article/pii/S0031938418300155.